# Thermoelectric transport of multi-Weyl semimetals in the quantum limit

L. X. Fu and C. M. Wang

# Thermoelectric transport of multi-Weyl semimetals in the quantum limit

L. X. Fu[1] and C. M. Wang[1, *]

[1]*Department of Physics, Shanghai Normal University, Shanghai 200234, China*
(Dated: December 6, 2021)

The thermoelectric transport properties of a three-dimensional multi-Weyl semimetal in the quantum limit are studied. In the calculation, we consider the different effects of the Gaussian and screened Coulomb electron-impurity scatterings. When the magnetic field is parallel to the electric field or the temperature gradient, the magnetoresistivity is always negative, but the thermopower strongly depends on the scattering potentials and the monopole charge. In the perpendicular field configuration, the situation becomes complicated. For the low electron density case, the increasing magnetic field makes the longitudinal conductivity comparable to the Hall one, which breaks the continuous growth of the Seebeck and Nernst responses, especially for the large monopole charge one. The thermoelectric Hall conductivity still indicates a plateau feature, but its value is multiplied by the monopole charge. Whether the longitudinal thermoelectric conductivity increases with the field depends on the potential type. This may be used to unveil the scattering mechanism in multi-Weyl semimetals.

## I. INTRODUCTION

Three-dimensional Weyl semimetals are a newly-discovered member of the topological materials family [1–7]. Its low energy excitation is depicted by the Weyl equation corresponding to a pair of particles with opposite chirality [8]. Each Weyl node carries a monopole charge $n$ in the momentum space. For a single-Weyl semimetal ($n = 1$), the dispersion near the Weyl nodes is linear in all three dimensions. However, there is no restriction on the charge of this monopole in condensed matter physics [9]. The so-called multi-Weyl semimetals possessing topological charge $n > 1$ have been recently proposed in $HgCr_2Se_4$ [2, 10], $SrSi_2$ [11, 12], $Cu_2Se$ and $RhAs_3$ [13]. The dispersion is still linear along a certain direction, but is nonlinear along the other two directions near the intersection points of the conduction and valence bands. This leads to strong anisotropy in the unique collective mode [14], optical [15–17] and quantum transport properties [18, 19].

The magnetic field is believed to be an effective means to tune the electrons in materials. There are many exotic magnetotransport phenomena in single-Weyl semimetals [20], including but not limited to negative magnetoresistivity arising from the chiral anomaly [21–24], the anomalous phase shift in the quantum oscillation [25], and the quantum oscillation or three-dimensional quantum Hall effect due to the Fermi arcs [26–29]. Researchers found that the monopole charge in multi-Weyl semimetals can alter these magnetotransport properties dramatically. The weak-field magnetoconductivity via quantum interference is normal to $+\sqrt{B}$ in double-Weyl semimetals [30], not $-\sqrt{B}$ in single-Weyl ones. The longitudinal magnetoconductivity and planar Hall conductivity scale cubically with the charge [31, 32]. The situation may become more sensitive when the magnetic field is so

strong that the system is in the quantum limit, where all the electrons occupy the lowest Landau band. Recently, novel phenomena of topological semimetals in the quantum limit have been discovered [33, 34]. Hence, the investigation of the quantum-limit magnetotransport in multi-Weyl semimetals is desirable.

The thermoelectric quantities may be influenced by the external field dramatically in contrast to the electric ones since they usually relate to the derivative of the chemical potential [35]. Therefore, the thermoelectric transport properties in multi-Weyl semimetals have attracted great attention [18, 31, 32, 36–39]. Especially, in the quantum limit there are some fascinating thermoelectric transport properties for single-Weyl or Dirac semimetals. When the magnetic field is perpendicular to the temperature gradient, the thermopower or the Nernst coefficient is non-saturating at this extreme field strength in this system in contrast to the usual Schrödinger particles [40–42]. Further, it is demonstrated that the thermoelectric Hall coefficient acquires a quantized value [43] in the quantum limit for this field configuration. Experimentally, these two relevant effects are observed in TaP [44] and $ZrTe_5$ [45, 46]. We find that in these studies the magnetic field is perpendicular to the electric field or the temperature gradient. The situation may be completely different when the magnetic field is parallel to the temperature gradient. Moreover, the effects of the scattering mechanism and the monopole charge on these thermoelectric quantities have not been investigated so far.

The outline of this paper is as follows. We start by giving the Landau bands of the three-dimensional multi-Weyl semimetal in Sec. II. In Sec. III, by considering the Gaussian and screened Coulomb potentials, the resistivity, thermoelectric conductivity and the Seebeck coefficient are calculated when the magnetic field is parallel to the electric field or the temperature gradient. Then we switch to the field configuration when the magnetic field is perpendicular to the electric field or the temperature gradient in Sec. IV. We compute the resistivities $\rho_{xx}$, $\rho_{xy}$, the thermoelectric conductivities $\alpha_{xx}$, $\alpha_{xy}$, the

Seebeck and Nernst coefficients. Finally, we present our conclusions in Sec. V.

## II. HAMILTONIAN AND THE LANDAU BANDS

We consider a three-dimensional multi-Weyl semimetal with the monopole charge $n$. The minimal Hamiltonian can be expressed with the form

$$H = \begin{bmatrix} H_+ & 0 \\ 0 & H_- \end{bmatrix}, \tag{1}$$

where $H_\chi$ is the single-particle Hamiltonian with the chirality $\chi = \pm 1$. Generally, it is given by [38, 39]

$$H_\chi = \chi v_n \boldsymbol{N_k} \cdot \boldsymbol{\sigma} + t_\chi (k_z - \chi k_W), \tag{2}$$

with

$$\boldsymbol{N_k} = \left[ k_\parallel^n \cos(n\xi), k_\parallel^n \sin(n\xi), (v/v_n)(k_z - \chi k_W) \right]. \tag{3}$$

Here $v_n$ is regarded as the general Fermi velocity in the $x$-$y$ plane, $v$ is the Fermi velocity along the z-direction, $t_\chi$ describes the tilt of the $\chi$ branch, $\boldsymbol{\sigma} = (\sigma_x, \sigma_y, \sigma_z)$ are three $2 \times 2$ Pauli matrices, $\boldsymbol{k} = (k_x, k_y, k_z)$ is the wave vector, $k_\parallel = \sqrt{k_x^2 + k_y^2}$, and $\xi = \tan^{-1}(k_y/k_x)$. The dispersion of the system can be obtained as

$$\varepsilon_{\chi\lambda} = \lambda\sqrt{v_n^2 k_\parallel^{2n} + v^2(k_z - \chi k_W)^2} + t_\chi(k_z - \chi k_W), \tag{4}$$

which bears two tilted cones with two Weyl nodes located at $(0, 0, \chi k_W)$, respectively. The quantum number $\lambda = \pm 1$ denotes the conduction (valence) bands. The $2k_W$ is the distance between the Weyl points in momentum space along the z-direction. We find that the tilts break the axial symmetry around the $k_z$ axis.

Now we assume the magnetic field applied along the z-direction $\boldsymbol{B} = B\hat{z}$, the Landau gauge is taken as $\boldsymbol{A} = -By\hat{x}$. Under the Peierls substitution $\boldsymbol{k} \to \boldsymbol{k} + e\boldsymbol{A}/\hbar$ with $-e$ being the charge of an electron, the Hamiltonian of the $\chi$ chirality is shown as the following form:

$$H_\chi = \begin{bmatrix} (\chi v + t_\chi)(k_z - \chi k_W) & \chi v_n(\hat{k}_x - i\hat{k}_y)^n \\ \chi v_n(\hat{k}_x + i\hat{k}_y)^n & (-\chi v + t_\chi)(k_z - \chi k_W) \end{bmatrix}, \tag{5}$$

with $\hat{k}_x = k_x - y/\ell_B^2$, $\hat{k}_y = -i\partial_y$ and $\ell_B = \sqrt{\hbar/eB}$ being the magnetic length. The Hamiltonian depends on the magnetic field through $B$. We can introduce two ladder operators $a^\dagger = (\ell_B/\sqrt{2})(k_x - y/\ell_B^2 + \partial_y)$ and $a = (\ell_B/\sqrt{2})(k_x - y/\ell_B^2 - \partial_y)$, which satisfy $[a, a^\dagger] = 1$. Then the above single Hamiltonian is rewritten as

$$H_\chi = \begin{bmatrix} (\chi v + t_\chi)(k_z - \chi k_W) & \chi\omega_n a^n \\ \chi\omega_n(a^\dagger)^n & (-\chi v + t_\chi)(k_z - \chi k_W) \end{bmatrix}, \tag{6}$$
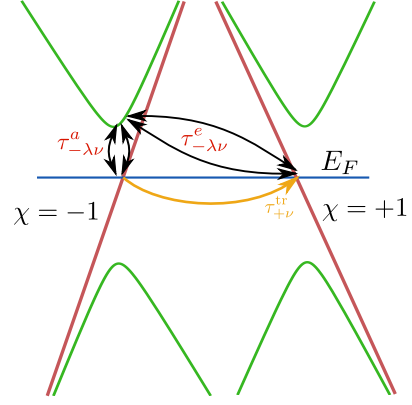


FIG. 1. The schematic diagram of the Landau bands for this multi-Weyl semimetals. $E_F$ is the Fermi energy, which only cuts the brown lowest bands in the quantum limit. $\tau_{+\nu}^{\mathrm{tr}}$ is the transport time described by Eq. (22). $\tau_{-\lambda\nu}^a$ and $\tau_{-\lambda\nu}^e$ are the intra-band and inter-band contributions of the lifetime due to the virtual processes going back and forth between the lowest bands $\chi'\nu'$ and the nearest ones $-\lambda\nu$.

with $\omega_n = v_n(\sqrt{2}/\ell_B)^n$. Then, the Landau energies and wavefunctions of total Hamiltonian $H$ for the Landau index $\nu \geq n$ are

$$E_{\chi\lambda\nu} = \lambda\sqrt{\frac{\nu!}{(\nu-n)!}\omega_n^2 + v^2(k_z - \chi k_W)^2} + t_\chi(k_z - \chi k_W), \tag{7}$$

$$\Psi_{+\lambda\nu} = \begin{bmatrix} \psi_{+\lambda\nu} \\ 0 \end{bmatrix}, \Psi_{-\lambda\nu} = \begin{bmatrix} 0 \\ \psi_{-\lambda\nu} \end{bmatrix}, \tag{8}$$

while for $0 \leq \nu < n$, they are

$$E_{\chi\nu} = -\chi v(k_z - \chi k_W) + t_\chi(k_z - \chi k_W), \tag{9}$$

$$\Psi_{+\nu} = \begin{bmatrix} \psi_{+\nu} \\ 0 \end{bmatrix}, \Psi_{-\nu} = \begin{bmatrix} 0 \\ \psi_{-\nu} \end{bmatrix}. \tag{10}$$

Here

$$\psi_{\chi\lambda\nu} = \frac{e^{i(k_x x + k_z z)}}{\sqrt{L_x L_z}}\begin{bmatrix} \sin\frac{\gamma}{2}\phi_{\nu-n} \\ \cos\frac{\gamma}{2}\phi_\nu \end{bmatrix}, \tag{11}$$

$$\psi_{\chi\nu} = \frac{e^{i(k_x x + k_z z)}}{\sqrt{L_x L_z}}\begin{bmatrix} 0 \\ \phi_\nu \end{bmatrix}, \tag{12}$$

with $L_x L_z$ being the area of the sample. $\gamma$ is determined by

$$\tan\frac{\gamma}{2} = \frac{\chi\omega_n\sqrt{\frac{\nu!}{(\nu-n)!}}}{\lambda\sqrt{\frac{\nu!}{(\nu-n)!}\omega_n^2 + v^2(k_z - \chi k_W)^2} - \chi v(k_z - \chi k_W)}.$$

And $\phi_\nu$ is the usual harmonic oscillator eigenstates at the center $y_0 = k_x\ell_B^2$ relating to the Hermite polynomials

$\mathcal{H}_\nu$

$$\phi_\nu(k_x, y) = \frac{1}{\sqrt{\sqrt{\pi}2^\nu\nu!\ell_B}}e^{-[(y-y_0)^2/2\ell_B^2]}\mathcal{H}_\nu\left(\frac{y-y_0}{\ell_B}\right). \tag{13}$$

For monopole charge $n = 1$, the above Landau bands reduce to the one in literature, such as [25, 47]. Similar to the $n = 1$ case, the lowest band $E_{\chi\nu}$ also linearly depends on $k_z$. Further, it is irrespective of the monopole charge showing $n$-fold degeneracy in contrast to the single Weyl case. The wavefunction of the lowest bands relies on the monopole charge through the index of the harmonic oscillator eigenstate. Fig. 1 indicates the Landau bands of this system. Clearly, the parameter $\chi$ indicates the chirality. We consider the quantum limit, where the magnetic field is extremely large that the Fermi energy only cuts the linear bands of opposite chiralities.

## III. LONGITUDINAL CONFIGURATION

We first consider that both the magnetic field and the electric field or the temperature gradient are along the $z$-direction, $\boldsymbol{B} \parallel \boldsymbol{E} \parallel \nabla T \parallel \hat{z}$, which is called the longitudinal configuration. The temperature is assumed to be very close to zero. We concentrate on the resistivity $\rho_{zz}$, thermoelectric conductivity $\alpha_{zz}$, and the Seebeck coefficient $S_{zz}$. The Mott relation is proved to be valid for the diagonal transport quantities [48]. Hence, these three transport quantities all relate to the conductivity $\sigma_{zz}$. From the Mott relation, we have [48–51]

$$\alpha_{zz} = -\frac{\pi^2 k_B^2 T}{3e}\frac{\partial\sigma_{zz}}{\partial E_F}, \tag{14}$$

$\rho_{zz} = 1/\sigma_{zz}$ and $S_{zz} = \alpha_{zz}/\sigma_{zz}$. Here $k_B$ is the Boltzmann constant, $T$ is the temperature, and $E_F$ is the Fermi energy.

When both fields are along the $z$-direction, by using the Greens function the electric conductivity $\sigma_{zz}$ can be derived from the standard Kubo formula [52, 53]. In the quantum limit, the Fermi energy is close to the charge neutrality point. However, we assume the scattering is so weak that $E_F\tau \gg 1$ is satisfied with $\tau$ being a certain relaxation time. The products of two retarded or advanced Green's functions could be neglected since they are smaller than the product of the retarded and advanced ones. Then the conductivity is

$$\sigma_{zz} = \frac{\hbar e^2}{2\pi V}\int d\varepsilon\left[-\frac{\partial n_F(\varepsilon)}{\partial\varepsilon}\right]\text{Tr}\left[\hat{v}_z\hat{G}^A(\varepsilon)\hat{v}_z\hat{G}^R(\varepsilon)\right]. \tag{15}$$

Here $V$ is the volume, $n_F(\varepsilon)$ is the Fermi-Dirac distribution function, $\hat{G}^{R/A}(\varepsilon)$ is the retarded (advanced) Green's function and $\hat{v}_z$ is the $z$-component of the veloc-

ity operator with

$$\hat{v}_z = \frac{1}{\hbar}\frac{\partial H}{\partial k_z} = \frac{1}{\hbar}\begin{bmatrix}\frac{\partial H_+}{\partial k_z} & 0 \\ 0 & \frac{\partial H_-}{\partial k_z}\end{bmatrix}. \tag{16}$$

In the quantum limit, the magnetic field is so strong that the Fermi energy only cuts the lowest Landau band $E_{\chi\nu}$. Hence, bearing in mind the Landau degeneracy $1/(2\pi\ell_B^2)$, the $\sigma_{zz}$ is given by

$$\sigma_{zz} = \frac{\hbar e^2}{4\pi^2\ell_B^2 L_z}\int d\varepsilon\left[-\frac{\partial n_F(\varepsilon)}{\partial\varepsilon}\right]\sum_{\chi,\nu,k_z}\left(v_\chi^z G_{\chi\nu}^A v_\chi^z G_{\chi\nu}^R\right), \tag{17}$$

with

$$v_\chi^z = \langle\Psi_{\chi\nu}|\hat{v}_z|\Psi_{\chi\nu}\rangle = \frac{1}{\hbar}(-\chi v + t_\chi), \tag{18}$$

$$G_{\chi\nu}^{R/A} = \langle\Psi_{\chi\nu}|\hat{G}^{R/A}|\Psi_{\chi\nu}\rangle = \frac{1}{\varepsilon - E_{\chi\nu} \pm i\frac{\hbar}{2\tau_{\chi\nu}}}. \tag{19}$$

Here $\tau_{\chi\nu}$ is the relaxation time. Using the identity

$$G_{\chi\nu}^R G_{\chi\nu}^A \simeq \frac{2\pi\tau_{\chi\nu}}{\hbar}\delta(\varepsilon - E_{\chi\nu}), \tag{20}$$

and at low temperature $-\partial n_F(\varepsilon)/\partial\varepsilon \simeq \delta(\varepsilon - E_F)$, the $\sigma_{zz}$ can be simplified. Further, it is proved that the relaxation time should be changed into the transport time $\tau_{\chi\nu}^{\text{tr}}$ at the Fermi energy when we consider the vertex correction of the velocity [52, 54]. Finally, the longitudinal conductivity is

$$\sigma_{zz} = \frac{e^2}{h}\frac{1}{2\pi\ell_B^2}\sum_{\chi,\nu}|\chi v - t_\chi|\frac{\tau_{\chi\nu}^{\text{tr}}}{\hbar}. \tag{21}$$

There is an additional factor $\left(1 - v_{\chi'}^z/v_\chi^z\right)$ in the transport time compared to the relaxation time given by the Fermi golden rule

$$\frac{\hbar}{\tau_{\chi\nu}^{\text{tr}}} = 2\pi\sum_{\chi',\nu',k_x',k_z'}\left\langle\left|U_{k_x,k_F^\chi;k_x',k_z'}^{\chi\nu,\chi'\nu'}\right|^2\right\rangle_{\text{imp}}\left(1 - \frac{v_{\chi'}^z}{v_\chi^z}\right)$$
$$\times \delta\left[E_F - E_{\chi'\nu'}(k_z')\right], \tag{22}$$

with $\left\langle\left|U_{k_x,k_z;k_x',k_z'}^{\chi\nu,\chi'\nu'}\right|^2\right\rangle_{\text{imp}}$ being the scattering matrix element after the impurity average [48] and $k_F^\chi$ being the Fermi wave vector of the $\chi$ branch determined by

$$k_F^\chi = -\frac{E_F}{\chi v - t_\chi} + \chi k_W. \tag{23}$$

The factor $\left(1 - v_{\chi'}^z/v_\chi^z\right)$ makes the $\chi' = \chi$ contribution of the transport time vanish. This means $\tau_{\chi\nu}^{\text{tr}}$ relates to the inter-chirality electron-impurity scattering displayed clearly in Fig. 1. For a constant transport time, the conductivity $\sigma_{zz}$ is proportional, and then the resistivity $\rho_{xx}$ is inversely proportional to the magnetic field. The

thermoelectric coefficients $\alpha_{zz}$ and $S_{zz}$ equal zero exactly since the conductivity is irrelevant to the Fermi energy. Note that the transport time is calculated in the first Born approximation. The contributions of the higher order Born approximation and the crossed impurity lines could be neglected safely since they are small in the weak scattering limit [55].

It is well-known that the transport time is very sensitive to the scattering potential of materials [54]. Generally, it should include both intra-chirality and inter-chirality processes though only the inter-chirality one affects the transport time for the longitudinal configuration. The scattering potential is assumed to be

$$\mathcal{U}(\boldsymbol{r}) = \begin{bmatrix} U_a(\boldsymbol{r})\sigma_0 & U_e(\boldsymbol{r})\sigma_0 \\ U_e(\boldsymbol{r})\sigma_0 & U_a(\boldsymbol{r})\sigma_0 \end{bmatrix}. \tag{24}$$

Here $\sigma_0$ is the $2 \times 2$ identity matrix, $U_a(\boldsymbol{r})$ and $U_e(\boldsymbol{r})$ represent the intra-chirality and inter-chirality electron-impurity scatterings, respectively. We assume real scalar scattering potentials $U_a^*(\boldsymbol{r}) = U_a(\boldsymbol{r})$ and $U_e^*(\boldsymbol{r}) = U_e(\boldsymbol{r})$ having the form

$$U_{a/e}(\boldsymbol{r}) = \sum_i V_{\mathrm{imp}}^{a/e}(\boldsymbol{r} - \boldsymbol{R}_i), \tag{25}$$

with the impurities randomly distributed at $\boldsymbol{R}_i$. Here the superscripts $a$ and $e$ mean the intra- and inter-chirality ones. We consider two different nonmagnetic scattering potentials in this work: the Gaussian potential and the screened Coulomb potential, which are two common choices used in literatures [54, 56]. The random Gaussian potential is [54]

$$V_{\mathrm{imp}}^c(\boldsymbol{r} - \boldsymbol{R}_i) = \frac{u_0}{(d\sqrt{2\pi})^3} e^{-|\boldsymbol{r}-\boldsymbol{R}_i|^2/2d^2}, \tag{26}$$

where $c = a/e$, $u_0$ measures the scattering strength, and $d$ is a parameter that determines the range of the scattering potential. For the screened Coulomb potential,

$$V_{\mathrm{imp}}^c(\boldsymbol{r} - \boldsymbol{R}_i) = \frac{e^2}{4\pi\epsilon_0\epsilon_r |\boldsymbol{r}-\boldsymbol{R}_i|} e^{-\kappa|\boldsymbol{r}-\boldsymbol{R}_i|}, \tag{27}$$

with $\epsilon_r$ denoting the dielectric constant, and $\kappa$ being the inverse of the screening length, which is obtained from the standard random phase approximation [48]. Though both scattering potentials decay with the distance, the different $\boldsymbol{r}$-dependence will lead to different Fourier transforms [48] and field-dependence of the transport quantities.

For the Gaussian potential, if we define $V_{\mathrm{G}}^e = n_{ei}u_0^2$ with $n_{ei}$ being the impurity density of the inter-chirality Gaussian scatterers, then the transport time is

$$\frac{\hbar}{\tau_{\chi\nu}^{\mathrm{tr}}} = \frac{V_{\mathrm{G}}^e}{2\pi\ell_B^2} e^{-4p_\chi^2 d^2} \frac{2\chi v + t_{\bar{\chi}} - t_\chi}{(\chi v - t_\chi)|\bar{\chi}v - t_{\bar{\chi}}|}$$
$$\times \sum_{\nu'<n} \frac{(n_1+n_2)!}{n_1!n_2!} \frac{(b-1)^{2n_2}}{b^{n_1+n_2+1}}$$
$$\times F\left[-n_2, -n_2; -n_1 - n_2; \frac{b(b-2)}{(b-1)^2}\right]. \tag{28}$$

Here $F(\alpha, \beta; \gamma; z)$ is the (Gauss) hypergeometric function, $\bar{\chi} = -\chi$, $n_1 = \max(\nu, \nu')$, $n_2 = \min(\nu, \nu')$, the parameter $b = 1 + 2d^2/\ell_B^2$, and

$$p_\chi = -\frac{1}{2}\left(\frac{E_F}{\chi v - t_\chi} + \frac{E_F}{\chi v + t_{\bar{\chi}}}\right) + \chi k_W. \tag{29}$$

Then the conductivity could be obtained with the help of Eq. (21). As $d \to 0$, $V_{\mathrm{imp}}^c(\boldsymbol{r} - \boldsymbol{R}_i) \to u_0\delta(\boldsymbol{r} - \boldsymbol{R}_i)$ turning into the $\delta$-form short-range scattering. The transport time reduces to

$$\frac{\hbar}{\tau_{\chi\nu}^{\mathrm{tr}}} = \frac{nV_{\mathrm{G}}^e}{2\pi\ell_B^2} \frac{2\chi v + t_{\bar{\chi}} - t_\chi}{(\chi v - t_\chi)|\bar{\chi}v - t_{\bar{\chi}}|}. \tag{30}$$

Therefore, the conductivity has the form

$$\sigma_{zz} = \frac{e^2}{h} \frac{1}{V_{\mathrm{G}}^e} \sum_\chi |\chi v - t_\chi| \frac{(\chi v - t_\chi)|\bar{\chi}v - t_{\bar{\chi}}|}{2\chi v + t_{\bar{\chi}} - t_\chi}, \tag{31}$$

which is independent of the magnetic field and the Fermi energy. Surprisingly, this result is irrespective of the monopole charge. Without tilting $t_\chi = 0$, it reduces to

$$\sigma_{zz} = \frac{e^2}{h} \frac{v^2}{V_{\mathrm{G}}^e}. \tag{32}$$

We get back to the same result in earlier work [53].

As long as $d \neq 0$, the conductivity $\sigma_{zz}$, the resistivity $\rho_{zz}$, and the thermoelectric conductivity $\alpha_{zz}$ depend on the monopole charge and the magnetic field. It is noted that since the $\nu'$-summation of the transport time Eq. (28) is independent of the chirality and only $p_\chi$ relies on the Fermi energy, the Seebeck coefficient $S_{zz}$ under the Gaussian potential is irrespective of the magnetic field $\boldsymbol{B}$ for fixed Fermi energy. Without tilts, $S_{zz}$ is given by

$$S_{zz} = \frac{\pi^2 k_B^2 T}{3e} \frac{8d^2}{v^2}(vk_W - E_F). \tag{33}$$

Usually, the total electron density $N_e$ is fixed in a neutral solid. Then the Fermi energy changes with the field. In the quantum limit, the Fermi energy reduces as the field rises

$$E_F = \frac{(2\pi)^2\ell_B^2 N_e}{n\sum_\chi \frac{1}{v-\chi t_\chi}} + \Lambda, \tag{34}$$

which is inversely proportional to the monopole charge with $\Lambda$ being the minimum energy. Hence, for the fixed electron density case, Seebeck response will depend on the magnetic field through the magnetic-field-dependent Fermi energy.

Now we move to the analysis of the screened Coulomb potential. In this case, the transport time is

$$\frac{\hbar}{\tau_{\chi\nu}^{\mathrm{tr}}} = \frac{V_{\mathrm{G}}^e\ell_B^2}{8\pi} \frac{2\chi v + t_{\bar{\chi}} - t_\chi}{(\chi v - t_\chi)|\bar{\chi}v - t_{\bar{\chi}}|} \sum_{\nu'} \frac{n_2!}{n_1!}$$
$$\times \int_0^\infty d\zeta \frac{\zeta^{n_1-n_2}e^{-\zeta}}{[\zeta + (4p_\chi^2 + \kappa^2)\ell_B^2/2]^2} \left[L_{n_2}^{n_1-n_2}(\zeta)\right]^2, \tag{35}$$

where $V_C^e = n_{ei}e^4/(\epsilon_0^2\epsilon_r^2)$ and $L_m^n(x)$ is the associated Laguerre polynomial. Here the summation of the $\tau_{\chi\nu}^{\mathrm{tr}}$ is in connection with the chirality, hence the $B$-dependence of the Seebeck response cannot be canceled through the division $\alpha_{zz}/\sigma_{zz}$ even for the fixed Fermi energy case.

The lowest magnetic field of the quantum limit $B_Q$ of the electron conduction corresponds to the case where the Fermi energy cuts the band bottom of $E_{\chi+n}$,

$$E_{\chi+n}|_{\min} = \frac{\sqrt{n!}\omega_n}{v}\sqrt{v^2 - t_\chi^2} = E_F. \qquad (36)$$

Specifically, the critical field without tilts is decided from

$$\sqrt{n!}\alpha_n(\sqrt{2}/\ell_{B_Q})^n = \frac{(2\pi)^2 v\ell_{B_Q}^2 N_e}{2n} + \Lambda, \qquad (37)$$

with $\ell_{B_Q} = \sqrt{\hbar/eB_Q}$. With the development of the technology for the material synthesis, the quantum limit could be realized at relatively low field. At $N_e = 10^{22}$ m$^{-3}$ (other needed parameters are listed in the caption of Fig. 2), $B_Q$ is about 5 T, which is achievable in experiments [47]. The corresponding maximum magnetic length is $\ell_{B_Q} \simeq 11.5$nm.

The numerically calculated electrical resistivity, the thermoelectric conductivity, and the Seebeck coefficient for various monopole charges as functions of the magnetic field are shown in Fig. 2, where $(a_i)$ and $(b_i)$ are for the Gaussian and the Coulomb potentials, respectively. In the following calculations, the minimum magnetic field is set to be 5 Tesla, above which the system is well in the quantum limit. As we can see from the figure, all the resistivities with different charges decrease with the magnetic field displaying the negative magnetoresistivity behavior for both scatterings. It is believed that the negative magnetoresistivity is regarded as the fingerprint of the Weyl semimetal. Here we demonstrated it is robust to the kind of the scattering and the monopole charge. In the Gaussian one, the remoter distance $d$ makes the scattering weaker, and then the resistivity decreases. However, the $\alpha_{zz}$ always increases with the field, which can be boosted by the disorder distance. More strikingly, the monopole charge influences the transport, which reduces the resistivity and enhances the thermoelectric conductivity for both two scattering cases. In the presence of Gaussian scattering, the Seebeck coefficient increases with field and nearly saturates at large field. The saturated values are proportional to $d^2$, which is consistent with the approximate equation (33). This is also valid for large distances [48]. The monopole charge somewhat enhances the $S_{zz}$. In contrast, the Seebeck response descends with the field and the monopole charge for the Coulomb impurity scattering. We then can deduce that the Seebeck $S_{zz}$ is very sensitive to the scattering potential and it can not realize the continuous growth in this longitudinal configuration. The ratios of these thermoelectric quantities could be seen in [48].
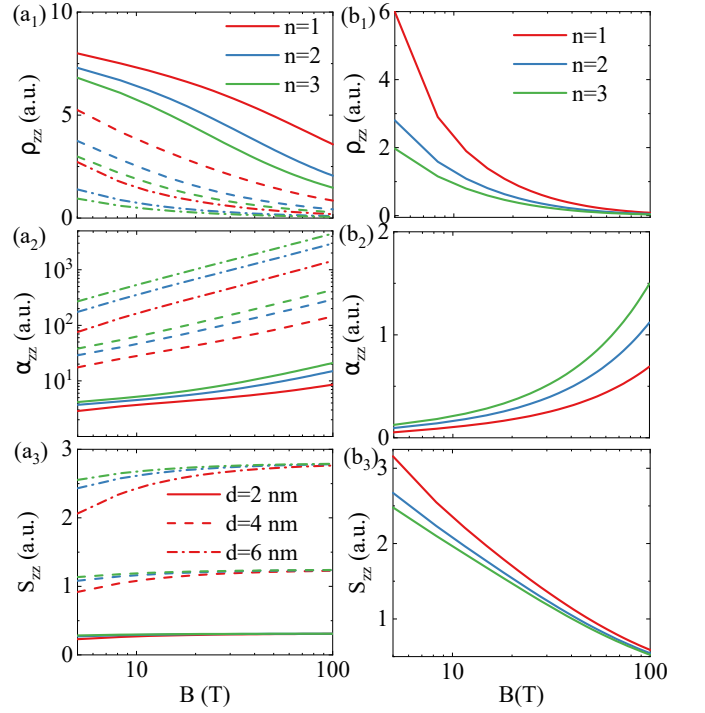


FIG. 2. The resistivity $\rho_{zz}$, the thermoelectric conductivity $\alpha_{zz}$, and the Seebeck coefficient of the multi-Weyl semimetals for the $\boldsymbol{B} \parallel \boldsymbol{E} \parallel \nabla T \parallel \hat{z}$ case as functions of magnetic field $\boldsymbol{B}$ under the Gaussian $(a_i)$ and screened Coulomb $(b_i)$ potentials for different monopole charges $n = 1$ (red), 2 (blue), 3 (green). Here $i = 1, 2, 3$. $d$ is a parameter that determines the range of the Gaussian scattering. $d = 2, 4, 6$ are displayed with solid, dash, and dash-dot lines. The values of the parameters are: $v = 0.1$ eVnm, $t_- = 0.01$ eVnm, $t_+ = 0.02$ eVnm, $k_W = 0.1$ nm$^{-1}$, $V_G^e = 10^{-4}$ eV$^2$nm$^3$, $V_C^e = 0.1$ eV$^2$/nm, $\epsilon_r = 10$, $\Lambda = 0$ and $N_e = 10^{22}$ m$^{-3}$.

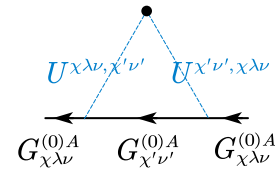## IV. TRANSVERSE CONFIGURATION



FIG. 3. The self-energy of the advanced Green's function $G_{\chi\lambda\nu}^A$. The Green's functions with the superscript (0) mean the bare ones.

The other field configuration frequently used experimentally is that the electric field (or the temperature gradient) and magnetic fields are normal to each other, which is called transverse configuration. We assume that the magnetic field is still along the $z$-direction. Since the $\hat{z}$-direction magnetic field quantizes the motion of electrons in the $x$-$y$ plane, the Landau bands only disperse with $k_z$. Hence, the diagonal element of $\hat{v}_x$ vanishes, completely. If the electric field is along the $x$ direction, there

will be a nonzero longitudinal conductivity $\sigma_{xx}$ along this direction, which relates to the higher-order off-diagonal velocity element. In single Weyl semimetals, it couples the zeroth Landau band with the first Landau band in the quantum limit. However, for the multi-Weyl case, the contributing velocity element couples the $E_{\chi\nu}$ bands with the higher bands $E_{\chi\lambda'\nu'}$, originating from the intra-chirality process,

$$
\begin{aligned}
v^{\chi x}_{\nu,\lambda'\nu'} &= \langle \Psi_{\chi\nu}(k_z) | \hat{v}_x | \Psi_{\chi\lambda'\nu'}(k_z) \rangle \\
&= \chi \frac{n\omega_n \ell_B}{\sqrt{2}\hbar} \sqrt{\frac{(\nu'-1)!}{(\nu'-n)!}} \sin\frac{\gamma_{\chi\lambda'\nu'}}{2} \delta_{\nu\nu'-1}.
\end{aligned}
\tag{38}
$$

Here $\delta_{\nu\nu'-1}$ is the Kronecker delta function. In the quantum limit, the conductivity $\sigma_{xx}$ is given by

$$
\begin{aligned}
\sigma_{xx} &= \frac{\hbar e^2}{2\pi L_z} \frac{1}{2\pi \ell_B^2} \int_{-\infty}^{\infty} d\varepsilon \left[ -\frac{\partial n_{\mathrm{F}}(\varepsilon)}{\partial \varepsilon} \right] \\
&\times \sum_{\chi,\nu<n,\lambda',\nu'\geq n,k_z} \mathrm{Re}\left[ (v^{\chi x}_{\nu,\lambda'\nu'})^2 G^A_{\chi\lambda'\nu'} G^R_{\chi\nu} \right],
\end{aligned}
\tag{39}
$$

where

$$
G^A_{\chi\lambda\nu} = \frac{1}{\varepsilon - E_{\chi\lambda\nu} - \Sigma^A_{\chi\lambda\nu}}.
$$

Since the Fermi energy only cuts the lowest bands $E_{\chi\nu}$, the self-energy is shown in Fig. 3 given by [53, 54, 57]

$$
\Sigma^A_{\chi\lambda\nu} = i \sum_{\chi',\nu'<n,k'_x,k'_z} \left\langle \left| U^{\chi\lambda\nu,\chi'\nu'}_{k_x,k_F^\chi;k'_x,k'_z} \right|^2 \right\rangle_{\mathrm{imp}} \mathrm{Im}G^{(0)A}_{\chi'\nu'},
$$

with the bare Green's function $G^{(0)A}_{\chi'\nu'} = 1/(\varepsilon - E_{\chi'\nu'} - i0^+)$. The self-energy can be calculated as

$$
\begin{aligned}
\Sigma^A_{\chi\lambda\nu} &= i\pi \sum_{\chi',\nu'<n,k'_x,k'_z} \left\langle \left| U^{\chi\lambda\nu,\chi'\nu'}_{k_x,k_F^\chi;k'_x,k'_z} \right|^2 \right\rangle_{\mathrm{imp}} \\
&\times \delta\left[ E_F - E_{\chi'\nu'}(k'_z) \right].
\end{aligned}
$$

Hence, the advanced Green's function $G^A_{\chi\lambda'\nu'}$

$$
G^A_{\chi\lambda'\nu'} = \frac{1}{\varepsilon - E_{\chi\lambda'\nu'} - i\frac{\hbar}{2\tau_{\chi\lambda'\nu'}}}.
\tag{40}
$$

The $\tau_{\chi\lambda\nu}$ is the lifetime due to the virtual process going back and forth between bands $E_{\chi'\nu'}$ and $E_{\chi\lambda\nu}$ with

$$
\begin{aligned}
\frac{\hbar}{\tau_{\chi\lambda\nu}} &\equiv \frac{\hbar}{\tau_{\chi\lambda\nu\leftrightarrow\chi'\nu'}}, \\
&= 2\pi \sum_{\chi',\nu'<n,k'_x,k'_z} \left\langle \left| U^{\chi\lambda\nu,\chi'\nu'}_{k_x,k_F^\chi;k'_x,k'_z} \right|^2 \right\rangle_{\mathrm{imp}} \\
&\times \delta\left[ E_F - E_{\chi'\nu'}(k'_z) \right].
\end{aligned}
\tag{41}
$$

In contrast to the longitudinal configuration where the transport time only relates to the inter-chirality process, both the intra- and inter-chirality processes contribute to the lifetime

$$
\frac{\hbar}{\tau_{\chi\lambda\nu}} = \frac{\hbar}{\tau^a_{\chi\lambda\nu}(0)} + \frac{\hbar}{\tau^e_{\chi\lambda\nu}(2p_\chi)}.
\tag{42}
$$

The lifetime due to the different process can be written in a unified form

$$
\begin{aligned}
\frac{\hbar}{\tau^c_{\chi\lambda\nu}(p)} &= n_{ci} \cos^2 \frac{\gamma_{\chi\lambda\nu}(k_F^\chi)}{2} \frac{1}{|v - \tilde{\chi}t_{\tilde{\chi}}|} \\
&\times \sum_{\nu'<n,q_x,q_y} |u_c(q_x,q_y,p)|^2 C_{\nu\nu'}(q_\parallel^2 \ell_B^2/2),
\end{aligned}
\tag{43}
$$

with

$$
C_{\nu\nu'}(\zeta) = \frac{n_2!}{n_1!} \zeta^{n_1-n_2} e^{-\zeta} \left[ L^{n_1-n_2}_{n_2}(\zeta) \right]^2.
\tag{44}
$$

Here $\tilde{\chi} = \chi$ when $c = a$, but $\tilde{\chi} = -\chi$ when $c = e$. $u_c(\boldsymbol{q})$ is the Fourier transform of the scattering potential $V^c_{\mathrm{imp}}(\boldsymbol{r})$, and $n_{ci}$ is the impurity density of the corresponding scatterers. These two virtual processes are displayed in Fig. 1 indicated by the black lines with arrows. At zero temperature, the conductivity $\sigma_{xx}$ can be simplified as

$$
\begin{aligned}
\sigma_{xx} &= \frac{\hbar e^2}{(2\pi)^2} \frac{1}{2\ell_B^2} \sum_{\chi,\lambda} \frac{(v^{\chi x}_{n-1,\lambda n})^2}{|\chi v - t_\chi|} \\
&\times \left. \frac{\frac{\hbar}{2\tau_{\chi\lambda n}}}{(E_F - E_{\chi\lambda n})^2 + \left(\frac{\hbar}{2\tau_{\chi\lambda n}}\right)^2} \right|_{k_z=k_F^\chi}.
\end{aligned}
\tag{45}
$$

The element $v^{\chi x}_{n-1,\lambda n}$ implies that the coupling between the lowest band $E_{\chi n-1}$ and the nearest high band $E_{\chi\lambda n}$ gives rise to the conductivity $\sigma_{xx}$ different from the single Weyl semimetal in the quantum limit [47, 53]. In the single Weyl semimetal, the velocity element couples the zeroth band to the first one. Hence, the conductivity of the multi-Weyl semimetals will strongly depends on the monopole charge.

Similarly, the conductivity $\sigma_{xx}$ for this $\boldsymbol{B} \parallel \hat{z}$ and $\boldsymbol{E} \parallel \hat{x}$ case also strongly depends on the scattering potential. The relaxation time for the Gaussian potential is calculated as [48]

$$
\begin{aligned}
\frac{\hbar}{\tau^c_{\chi\lambda\nu}(p)} &= \frac{V_{\mathrm{G}}^c}{2\pi\ell_B^2} e^{-p^2 d^2} \cos^2 \frac{\gamma_{\chi\lambda\nu}(k_F^\chi)}{2} \frac{1}{|v - \tilde{\chi}t_{\tilde{\chi}}|} \\
&\times \sum_{\nu'<n} \frac{(n_1+n_2)!}{n_1!n_2!} \frac{(b-1)^{2n_2}}{b^{n_1+n_2+1}} \\
&\times F\left[ -n_2,-n_2;-n_1-n_2;\frac{b(b-2)}{(b-1)^2} \right].
\end{aligned}
\tag{46}
$$

And for the screened Coulomb scattering, it is given by

$$
\frac{\hbar}{\tau_{\chi\lambda\nu}^c(p)} = \frac{V_C^c \ell_B^2}{8\pi} \cos^2 \frac{\gamma_{\chi\lambda\nu}(k_F^\chi)}{2} \frac{1}{|v - \tilde{\chi} t_{\tilde{\chi}}|}
$$
$$
\times \sum_{\nu' < n} \frac{n_2!}{n_1!} \int_0^\infty d\zeta \frac{\zeta^{n_1 - n_2} e^{-\zeta}}{[\zeta + (p^2 + \kappa^2)\ell_B^2/2]^2}
$$
$$
\times \left[ L_{n_2}^{n_1 - n_2}(\zeta) \right]^2. \tag{47}
$$

For this transverse configuration ($\boldsymbol{B} \parallel \hat{z}$ and $\boldsymbol{E} \parallel \hat{x}$), there also exist the Hall conductivity $\sigma_{yx}$. For this three-dimensional system dispersing with $k_z$, it is known that each $k_z$ contributes a quantized Hall conductance $e^2/h$, hence the total Hall conductivity is [53]

$$
\sigma_{yx} = \sum_{\chi, \nu} (-\chi) \int_{k_{\text{cut}}^\chi}^{k_F^\chi} \frac{dk_z}{2\pi} \frac{e^2}{h}. \tag{48}
$$

Here $k_{\text{cut}}^\chi = -\Lambda/(\chi v - t_\chi) + \chi k_W$ is the cut-off of the $k_z$. We can deduce that

$$
\sigma_{yx} = n \frac{e^2}{2\pi h} \sum_\chi \frac{E_F - \Lambda}{v - \chi t_\chi}. \tag{49}
$$

With the help of the expression of the electron density at zero temperature $N_e = \sum_{\chi, \nu < n} \sum_{k_x, k_z} \Theta(E_F - E_{\chi\nu}) = n \frac{1}{(2\pi)^2 \ell_B^2} \sum_\chi (-\chi)(k_F^\chi - k_{\text{cut}}^\chi)$, it could be found that the above Hall conductivity $\sigma_{yx} = eN_e/B$, this is the well-known classical Hall conductivity. Note that the Hall conductivity is calculated in the dissipationless limit since the disorder plays higher order contribution. Moreover, the resistivities $\rho_{xx}$ and $\rho_{xy}$ can be written as

$$
\rho_{xx} = \frac{\sigma_{xx}}{\sigma_{xx}^2 + \sigma_{yx}^2}, \tag{50}
$$

$$
\rho_{xy} = -\rho_{yx} = \frac{\sigma_{yx}}{\sigma_{xx}^2 + \sigma_{yx}^2}. \tag{51}
$$

In the presence of $\boldsymbol{B} \parallel \hat{z}$ and $-\nabla T \parallel \hat{x}$, the total current is $\boldsymbol{J} = \boldsymbol{\sigma} \cdot \boldsymbol{E} + \boldsymbol{\alpha} \cdot (-\nabla T)$ with $\boldsymbol{\sigma}$ and $\boldsymbol{\alpha}$ being the conductivity and thermoelectric tensors. In the open-circuit situation ($\boldsymbol{J} = 0$), the temperature gradient leads to an electric field $\boldsymbol{E} = (E_x, E_y)$, then the Seebeck and Nernst coefficients are obtained as [35]

$$
S_{xx} = -E_x/|\nabla T| = \rho_{xx}\alpha_{xx} + \rho_{yx}\alpha_{xy}, \tag{52}
$$
$$
S_{xy} = E_y/|\nabla T| = \rho_{xx}\alpha_{xy} - \rho_{yx}\alpha_{xx}. \tag{53}
$$

The thermoelectric conductivity $\alpha_{ij}$ in the quantum limit can be obtained from [43, 58]

$$
\alpha_{xy} = \frac{2e}{h} \sum_{\chi, \nu, k_z} (-\chi) s \left( \frac{E_{\chi\nu} - \mu}{k_B T} \right),
$$

with $\mu$ being the chemical potential. Here the entropy per electron state equals to

$$
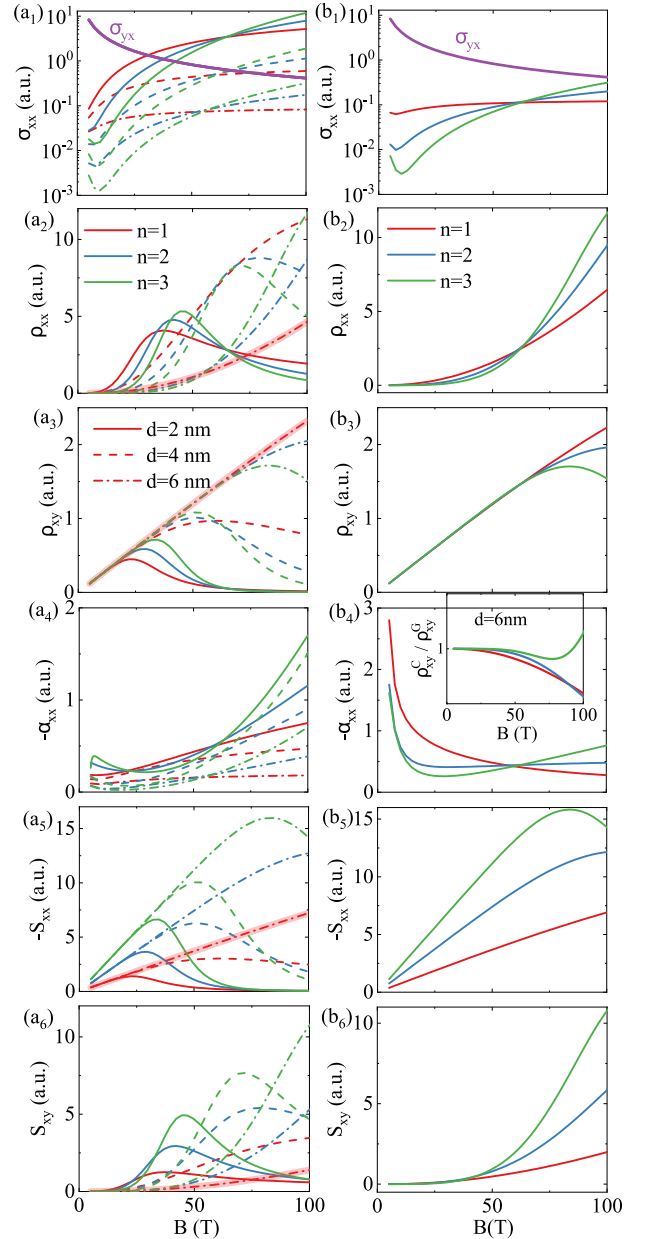s(x) = k_B \left[ \ln(1 + e^x) - \frac{x}{1 + e^{-x}} \right].
$$



FIG. 4. The conductivities, electrical resistivities $\rho_{xx}$ and $\rho_{xy}$, thermoelectric conductivity $\alpha_{xx}$, Seebeck coefficient $S_{xx}$, and Nernst coefficient $S_{xy}$ of the multi-Weyl semimetals as functions of magnetic field under Gaussian ($a_i$) and screened Coulomb ($b_i$) scatterings in the transverse $\boldsymbol{B} \parallel \hat{z}, \boldsymbol{E} \parallel \nabla T \parallel \hat{x}$ case. The inset of ($b_4$) indicates the ratio of the Hall resistivities due to the Coulomb potential and the Gaussian one. Here $\alpha = 0.05$ eVnm$^n$, $V_G^a = V_G^e = 10^{-4}$ eV$^2$nm$^3$, and $V_C^a = V_C^e = 0.1$ eV$^2$/nm. The other parameters are the same as Fig. 2.

At low temperature $\mu \gg k_B T$, the thermoelectric Hall conductivity then is found as

$$
\alpha_{xy} = \frac{\pi n e k_B^2 T}{6h} \sum_\chi \frac{1}{v - \chi t_\chi}, \tag{54}
$$

which is a constant independent of the magnetic field and the Fermi energy or the electron density. The result is in accordance with the one of Fu's group when $n = 1$ and without tilts [43]. For multi-Weyl semimetals, this constant thermoelectric Hall conductivity is proportional to the monopole charge. The coefficient $\sum_\chi \frac{1}{v - \chi t_\chi}$ could be found from the energy band calculation or the angle-resolved photoemission spectroscopy. Hence, the measurement of the $\alpha_{xy}$ in the quantum limit can be applied to determine the value of $n$.

For the given lifetimes due to different electron-impurity scatterings, the longitudinal conductivity $\sigma_{xx}$ could be obtained numerically. Then the resistivities $\rho_{xx}$ and $\rho_{xy}$, thermoelectric conductivity $\alpha_{xx}$, Seebeck and Nernst coefficients $S_{xx}$ and $S_{xy}$ are got, directly. For the Gaussian and the screened Coulomb potentials, these transport coefficients are depicted in Figs. 4 $(a_i)$ and $(b_i)$. In previous works [40, 41], $\sigma_{yx} \gg \sigma_{xx}$ is assumed, which leads to the nearly linear and non-saturating Seebeck coefficient. This assumption is valid in the dissipationless limit. In the dissipative case, this assumption means a large density, and then a very large $B_Q$ since $\sigma_{yx} \propto N_e$. For instance, the field $B_Q \simeq 40$ T for a massive Dirac semimetal having $N_e = 10^{24}$ m$^{-3}$ [41]. Nowadays this quantum limit field is not easily accessible, experimentally. Because of the low electron density used in our calculation ($N_e = 10^{22}$ m$^{-3}$), the value of the Hall conductivity $\sigma_{yx}$ is not always larger than the longitudinal one $\sigma_{xx}$. We can see this feature clearly in Fig. 4 $(a_1)$ for the Gaussian potential with $d = 2, 4$ nm. The competition between these two conductivities breaks the continuous growth of the Seebeck and Nernst coefficients due to the denominator in the resistivities $\sigma_{xx}^2 + \sigma_{yx}^2$. This low electron density or small $B_Q$ has been achieved, recently [47, 59].

Since $\tau_{\chi\lambda\nu}^c \propto e^{p^2 d^2}$ for the Gaussian scattering, the lifetime enhances drastically as the distance $d$ increases. It is due to the weakening of the scattering. Further, at this extremely large field, the Fermi energy only cuts the lowest band $E_{\chi\nu}$. The nearest band $E_{\chi\lambda n}$ is well above the Fermi energy, hence $|E_F - E_{\chi\lambda n}| \gg \hbar/\tau_{\chi\lambda\nu}^c$. Therefore, from the expression of $\sigma_{xx}$ Eq. (45), we can deduce $\sigma_{xx} \sim \hbar/\tau_{\chi\lambda\nu}^c \propto e^{-p^2 d^2}$. The smaller the distance is, the larger the conductance is. This is in vivid contrast to the longitudinal configuration $\boldsymbol{E} || \boldsymbol{B}$, where the conductivity is normal to the transport time, then the $\sigma_{zz}$ increases with the distance $d$. At the large distance $d = 6$ nm, the $\sigma_{xx}$ is smaller than the Hall conductivity for the single Weyl semimetal ($n = 1$). Hence, the usual linear Hall resistivity (the thick red line) could be seen in Fig. 4 $(a_3)$. In this situation, the longitudinal resistivity, Seebeck and Nernst responses increase monotonously shown with thick red lines in $(a_2)$, $(a_5)$, and $(a_6)$. If one reduces $d$, $\sigma_{xx}$ increases and becomes comparable to the $\sigma_{yx}$ leading to the nonlinear Hall resistivity because of the factor $\sigma_{xx}^2 + \sigma_{yx}^2$. Especially, at a very small distance $d = 2$ nm, the Hall resistivity shows a peak at near 20 T

shown with the red solid line in Fig. 4 $(a_3)$. This peak feature could also be seen in $\rho_{xx}$, $S_{xx}$, and $S_{xy}$ since they all depend on $\sigma_{xx}^2 + \sigma_{yx}^2$. The Seebeck and the Nernst coefficients may nearly decrease to zero in sharp contrast to Refs. [40, 41]. Moreover, the monopole charge could also somewhat enhance the longitudinal conductivity $\sigma_{xx}$ at large field. Hence, the continuous growth of the Seebeck and Nernst coefficients can be broken even at a large distance. The monopole charge could enhance the $S_{xx}$ and $S_{xy}$ at a fixed field. This competition could also be seen from the ratio of the Hall resistivities $\rho_{xy}^C/\rho_{xy}^G$ shown in the inset of $(b_4)$ with $\rho_{xy}^{C/G}$ being the Hall resistivity due to the Coulomb or Gaussian potential. At the small field, the ratio nearly equals one, which means the Hall conductivity dominates. With increasing the field, it departs from one since the conductivity $\sigma_{xx}$ becomes more and more important. This behavior could also be seen from the ratio of $S_{xx}$ [48].

For screened Coulomb impurity scattering, the behaviors of the $\rho_{xx}$, $\rho_{xy}$, $S_{xx}$, and $S_{xy}$ are qualitatively analogous to the ones for Gaussian potential at $d = 6$ nm. And the monopole charge affects them in a similar manner. This is due to the specific parameters used in this work for two potentials decaying with distance. However, the field-dependence of the thermoelectric conductivities for two potentials is completely different [see $(a_4)$ and $(b_4)$]. This is because that $\alpha_{xx}$ directly relates to the derivative of the Fermi energy, hence it is more sensitive to the scattering type. These two distinct behaviors of $\alpha_{xx}$ may help us to find out the type of the electron-impurity scattering in Weyl semimetals, which is still a challenging task in experiments.

Even for a constant lifetime, the competition between $\sigma_{xx}$ and $\sigma_{yx}$ may exist [48]. Hence, the resistivities, and the thermoelectric coefficients $S_{xx}$ and $S_{xy}$ will show peaks analogous to the Gaussian and screened Coulomb scatterings. However, the thermoelectric conductivity $\alpha_{xx}$ displays completely different behavior and it is also sensitive to the monopole charge.

## V. SUMMARY

In conclusion, we have investigated the thermoelectric transport of multi-Weyl semimetals in the quantum limit within the linear response theory. The dispersion becomes anisotropic if the topological charge $n > 1$. In the presence of the Gaussian potential and the screened Coulomb potential, we discuss two field configurations. One is the longitudinal configuration, where the magnetic field and the electric field or the temperature gradient are both along the $z$-direction. The other is the transverse one: the magnetic field is along the $z$-direction, but the electric field or the temperature gradient is along the $x$ direction.

In the longitudinal configuration, the resistivity shows the negative magnetoresistivity behavior for both two kinds of scattering potentials, which is also robust to

the monopole charge. The thermoelectric conductivity always increases with the field, which can be boosted by the disorder distance of the Gaussian potential. However, the behaviors of the Seebeck coefficient strongly rely on the scattering types. For the transverse configuration, the lifetime originates from the virtual intra- and inter-band scattering processes. We find that the non-saturating Seebeck and Nernst coefficients occur in the regime $\sigma_{yx} \gg \sigma_{xx}$. This condition is valid in the system with a large electron density resulting in a very large $B_Q$. For a small density system, the $B_Q$ is small, hence two conductivities $\sigma_{yx}$ and $\sigma_{xx}$ are comparable. This breaks the continuous growth of $S_{xx}$ and $S_{xy}$. It is obvious for

a system with a large monopole charge or a short-range scattering distance. Furthermore, the magnitude of $\alpha_{xx}$ increases with the magnetic field for the Gaussian scattering, but decreases for the Coulomb one. Our work may point out the route to search the materials with larger thermopower response.

[1] X. Wan, A. M. Turner, A. Vishwanath, and S. Y. Savrasov, Topological semimetal and Fermi-arc surface states in the electronic structure of pyrochlore iridates, Phys. Rev. B **83**, 205101 (2011).

[2] G. Xu, H. M. Weng, Z. J. Wang, X. Dai, and Z. Fang, Chern semimetal and the quantized anomalous Hall effect in HgCr$_2$Se$_4$, Phys. Rev. Lett. **107**, 186806 (2011).

[3] A. A. Burkov and L. Balents, Weyl semimetal in a topological insulator multilayer, Phys. Rev. Lett. **107**, 127205 (2011).

[4] H. M. Weng, C. Fang, Z. Fang, B. A. Bernevig, and X. Dai, Weyl semimetal phase in noncentrosymmetric transition-metal monophosphides, Phys. Rev. X **5**, 011029 (2015).

[5] B. Q. Lv, H. M. Weng, B. B. Fu, X. P. Wang, H. Miao, J. Ma, P. Richard, X. C. Huang, L. X. Zhao, G. F. Chen, Z. Fang, X. Dai, T. Qian, and H. Ding, Experimental discovery of Weyl semimetal TaAs, Phys. Rev. X **5**, 031013 (2015).

[6] N. P. Armitage, E. J. Mele, and A. Vishwanath, Weyl and Dirac semimetals in three-dimensional solids, Rev. Mod. Phys. **90**, 015001 (2018).

[7] B. Q. Lv, T. Qian, and H. Ding, Experimental perspective on three-dimensional topological semimetals, Rev. Mod. Phys. **93**, 025002 (2021).

[8] H. Weyl, Elektron und gravitation. I, Z. Physik **56**, 330 (1929).

[9] B.-J. Yang and N. Nagaosa, Classification of stable three-dimensional Dirac semimetals with nontrivial topology, Nat. Commun. **5**, 4898 (2014).

[10] C. Fang, M. J. Gilbert, X. Dai, and B. A. Bernevig, Multi-Weyl topological semimetals stabilized by point group symmetry, Phys. Rev. Lett. **108**, 266802 (2012).

[11] S.-M. Huang, S.-Y. Xu, I. Belopolski, C.-C. Lee, G. Chang, T.-R. Chang, B. Wang, N. Alidoust, G. Bian, M. Neupane, D. Sanchez, H. Zheng, H.-T. Jeng, A. Bansil, T. Neupert, H. Lin, and M. Z. Hasan, New type of Weyl semimetal with quadratic double Weyl fermions, Proc. Natl. Acad. Sci. USA **113**, 1180 (2016).

[12] B. Singh, G. Chang, T.-R. Chang, S.-M. Huang, C. Su, M.-C. Lin, H. Lin, and A. Bansil, Tunable double-Weyl fermion semimetal state in the SrSi$_2$ materials class, Sci. Rep. **8**, 10540 (2018).

[13] Z. Zhu, Y. Liu, Z.-M. Yu, S.-S. Wang, Y. X. Zhao, Y. Feng, X.-L. Sheng, and S. A. Yang, Quadratic contact point semimetal: Theory and material realization, Phys. Rev. B **98**, 125104 (2018).

[14] S. Ahn, E. H. Hwang, and H. Min, Collective modes in multi-Weyl semimetals, Sci. Rep. **6**, 34023 (2016).

[15] S. Ahn, E. J. Mele, and H. Min, Optical conductivity of multi-Weyl semimetals, Phys. Rev. B **95**, 161112(R) (2017).

[16] Y. Sun and A.-M. Wang, Magneto-optical conductivity of double Weyl semimetals, Phys. Rev. B **96**, 085147 (2017).

[17] S. P. Mukherjee and J. P. Carbotte, Doping and tilting on optics in noncentrosymmetric multi-Weyl semimetals, Phys. Rev. B **97**, 045150 (2018).

[18] S. Park, S. Woo, E. J. Mele, and H. Min, Semiclassical Boltzmann transport theory for multi-Weyl semimetals, Phys. Rev. B **95**, 161113(R) (2017).

[19] V. A. Zyuzin, Magnetotransport of Weyl semimetals due to the chiral anomaly, Phys. Rev. B **95**, 245128 (2017).

[20] H.-Z. Lu and S.-Q. Shen, Quantum transport in topological semimetals under magnetic fields, Front. Phys. **12**, 127201 (2017).

[21] H. J. Kim, K. S. Kim, J. F. Wang, M. Sasaki, N. Satoh, A. Ohnishi, M. Kitaura, M. Yang, and L. Li, Dirac versus Weyl fermions in topological insulators: Adler-Bell-Jackiw anomaly in transport phenomena, Phys. Rev. Lett. **111**, 246603 (2013).

[22] X. C. Huang, L. X. Zhao, Y. J. Long, P. P. Wang, D. Chen, Z. H. Yang, H. Liang, M. Q. Xue, H. M. Weng, Z. Fang, X. Dai, and G. F. Chen, Observation of the chiral-anomaly-induced negative magnetoresistance in 3D Weyl semimetal TaAs, Phys. Rev. X **5**, 031023 (2015).

[23] J. Xiong, S. K. Kushwaha, T. Liang, J. W. Krizan, M. Hirschberger, W. Wang, R. J. Cava, and N. P. Ong, Evidence for the chiral anomaly in the Dirac semimetal Na$_3$Bi, Science **350**, 413 (2015).

[24] Q. Li, D. E. Kharzeev, C. Zhang, Y. Huang, I. Pletikosic, A. V. Fedorov, R. D. Zhong, J. A. Schneeloch, G. D. Gu, and T. Valla, Chiral magnetic effect in ZrTe$_5$, Nat. Phys. **12**, 550 (2016).

[25] C. M. Wang, H.-Z. Lu, and S.-Q. Shen, Anomalous phase shift of quantum oscillations in 3D topological semimetals, Phys. Rev. Lett. **117**, 077201 (2016).

[26] A. C. Potter, I. Kimchi, and A. Vishwanath, Quantum

[27] P. J. W. Moll, N. L. Nair, T. Helm, A. C. Potter, I. Kimchi, A. Vishwanath, and J. G. Analytis, Transport evidence for Fermi-arc-mediated chirality transfer in the Dirac semimetal $Cd_3As_2$, Nature **535**, 266 (2016).

[28] C. M. Wang, H.-P. Sun, H.-Z. Lu, and X. C. Xie, 3D quantum Hall effect of Fermi arcs in topological semimetals, Phys. Rev. Lett. **119**, 136806 (2017).

[29] C. Zhang, Y. Zhang, X. Yuan, S. Lu, J. Zhang, A. Narayan, Y. Liu, H. Zhang, Z. Ni, R. Liu, E. S. Choi, A. Suslov, S. Sanvito, L. Pi, H.-Z. Lu, A. C. Potter, and F. Xiu, Quantum Hall effect based on Weyl orbits in $Cd_3As_2$, Nature **565**, 331 (2019).

[30] X. Dai, H.-Z. Lu, S.-Q. Shen, and H. Yao, Detecting monopole charge in Weyl semimetals via quantum interference transport, Phys. Rev. B **93**, 161110(R) (2016).

[31] R. M. A. Dantas, F. Peña-Benitez, B. Roy, and P. Surówka, Magnetotransport in multi-Weyl semimetals: a kinetic theory approach, J. High Energy Phys. **2018**, 69.

[32] T. Nag and S. Nandy, Magneto-transport phenomena of type-I multi-Weyl semimetals in co-planar setups, J. Phys.: Condens. Matter **33**, 075504 (2020).

[33] C. M. Wang, H.-Z. Lu, and X. C. Xie, Quantum oscillation beyond the quantum limit in pseudospin Dirac materials, Phys. Rev. B **102**, 041204(R) (2020).

[34] T. Devakul, Y. H. Kwan, S. L. Sondhi, and S. A. Parameswaran, Quantum Oscillations in the Zeroth Landau Level: Serpentine Landau Fan and the Chiral Anomaly, Phys. Rev. Lett. **127**, 116602 (2021).

[35] T. Liang, Q. Gibson, J. Xiong, M. Hirschberger, S. P. Koduvayur, R. J. Cava, and N. P. Ong, Evidence for massive bulk Dirac fermions in $Pb_{1-x}Sn_xSe$ from Nernst and thermopower experiments, Nat. Commun. **4**, 2696 (2013).

[36] Q. Chen and G. A. Fiete, Thermoelectric transport in double-Weyl semimetals, Phys. Rev. B **93**, 155125 (2016).

[37] E. V. Gorbar, V. A. Miransky, I. A. Shovkovy, and P. O. Sukhachov, Anomalous thermoelectric phenomena in lattice models of multi-Weyl semimetals, Phys. Rev. B **96**, 155138 (2017).

[38] A. Menon and B. Basu, Anomalous Hall transport in tilted multi-Weyl semimetals, J. Phys.: Condens. Matter **33**, 045602 (2020).

[39] T. Nag, A. Menon, and B. Basu, Thermoelectric transport properties of Floquet multi-Weyl semimetals, Phys. Rev. B **102**, 014307 (2020).

[40] B. Skinner and L. Fu, Large, nonsaturating thermopower in a quantizing magnetic field, Sci. Adv. **4**, eaat2621 (2018).

[41] V. Könye and M. Ogata, Thermoelectric transport coefficients of a Dirac electron gas in high magnetic fields, Phys. Rev. B **100**, 155430 (2019).

[42] I. Mandal and K. Saha, Thermopower in an anisotropic two-dimensional Weyl semimetal, Phys. Rev. B **101**, 045101 (2020).

[43] V. Kozii, B. Skinner, and L. Fu, Thermoelectric Hall conductivity and figure of merit in Dirac/Weyl materials, Phys. Rev. B **99**, 155123 (2019).

[44] F. Han, N. Andrejevic, T. Nguyen, V. Kozii, Q. T. Nguyen, T. Hogan, Z. Ding, R. Pablo-Pedro, S. Parjan, B. Skinner, A. Alatas, E. Alp, S. Chi, J. Fernandez-Baca, S. Huang, L. Fu, and M. Li, Quantized thermoelectric Hall effect induces giant power factor in a topological semimetal, Nat. Commun. **11**, 6167 (2020).

[45] W. Zhang, P. Wang, B. Skinner, R. Bi, V. Kozii, C.-W. Cho, R. Zhong, J. Schneeloch, D. Yu, G. Gu, L. Fu, X. Wu, and L. Zhang, Observation of a thermoelectric Hall plateau in the extreme quantum limit, Nat. Commun. **11**, 1046 (2020).

[46] P. Wang, C.-w. Cho, F. Tang, P. Wang, W. Zhang, M. He, G. Gu, X. Wu, Y. Shao, and L. Zhang, Giant Nernst effect and field-enhanced transversal $z_N$T in $ZrTe_5$, Phys. Rev. B **103**, 045203 (2021).

[47] J. L. Zhang, C. M. Wang, C. Y. Guo, X. D. Zhu, Y. Zhang, J. Y. Yang, Y. Q. Wang, Z. Qu, L. Pi, H.-Z. Lu, and M. L. Tian, Anomalous thermoelectric effects of $ZrTe_5$ in and beyond the quantum limit, Phys. Rev. Lett. **123**, 196602 (2019).

[48] See Supplemental Materials for the detailed calculations of the matrix elements of the scattering potentials, the Fourier transforms of the potentials, the derivation of the transport time and the lifetime, the derivation of the Mott relation for a general system, and some additional numerical results..

[49] Y. Ferreiros, A. A. Zyuzin, and J. H. Bardarson, Anomalous Nernst and thermal Hall effects in tilted Weyl semimetals, Phys. Rev. B **96**, 115202 (2017).

[50] M. Jonson and G. D. Mahan, Mott's formula for the thermopower and the Wiedemann-Franz law, Phys. Rev. B **21**, 4223 (1980).

[51] R. Lundgren, P. Laurell, and G. A. Fiete, Thermoelectric properties of Weyl and Dirac semimetals, Phys. Rev. B **90**, 165115 (2014).

[52] G. D. Mahan, *Many-Particle Physics* (Plenum Press, 1990).

[53] H. Z. Lu, S. B. Zhang, and S. Q. Shen, High-field magnetoconductivity of topological semimetals with short-range potential, Phys. Rev. B **92**, 045203 (2015).

[54] S.-B. Zhang, H.-Z. Lu, and S.-Q. Shen, Linear magneto-conductivity in an intrinsic topological Weyl semimetal, New J. Phys. **18**, 053039 (2016).

[55] H. Bruus and K. Flensberg, *Many-Body Quantum Theory in Condensed Matter Physics: An Introduction* (Oxford Graduate Texts, 2004).

[56] Y. Chen, H.-Z. Lu, and X. C. Xie, Forbidden backscattering and resistance dip in the quantum limit as a signature for topological insulators, Phys. Rev. Lett. **121**, 036602 (2018).

[57] A. A. Abrikosov, Quantum magnetoresistance, Phys. Rev. B **58**, 2788 (1998).

[58] D. L. Bergman and V. Oganesyan, Theory of dissipationless Nernst effects, Phys. Rev. Lett. **104**, 066601 (2010).

[59] F. Tang, Y. Ren, P. Wang, R. Zhong, J. Schneeloch, S. A. Yang, K. Yang, P. A. Lee, G. Gu, Z. Qiao, and L. Zhang, Three-dimensional quantum Hall effect and metal-insulator transition in $ZrTe_5$, Nature **569**, 537 (2019).